Science of the Total Environment 826 (2022) 153692

Contents lists available at ScienceDirect

Science of the Total Environment

journal homepage: www.elsevier.com/locate/scitotenv

Nitrous acid in the polluted coastal atmosphere of the South China Sea: Ship emissions, budgets, and impacts

Rongrong Gu [a,b], Weihao Wang [b,c], Xiang Peng [b,d], Men Xia [b], Min Zhao [a], Yingnan Zhang [a], Ya'nan Wang [b], Yiming Liu [e], Hengqing Shen [a], Likun Xue [a,f,*], Tao Wang [b,a,*], Wenxing Wang [a]

[a] Environment Research Institute, Shandong University, Qingdao 266237, China
[b] Department of Civil and Environmental Engineering, The Hong Kong Polytechnic University, Hong Kong 999077, China
[c] Hangzhou PuYu Technology Development Co., Ltd, Hangzhou 311300, China
[d] Department of Ambient Air Quality Monitoring, China National Environmental Monitoring Center, Beijing 100012, China
[e] School of Atmospheric Sciences, Sun Yat-sen University, Zhuhai 519082, China
[f] Collaborative Innovation Center for Climate Change, Nanjing, Jiangsu 210023, China

HIGHLIGHTS

- The ship emission ratio of HONO/NO_x is 1.21 ± 0.99%.
- The offshore sea is badly impacted by human activities and serves as an HONO sink.
- NO_2 conversion and TNO_3 photolysis dominate HONO production in coastal air.
- NO_x-related sources dominate HONO production in continental air.
- HONO contributes to increasing AOC in marine, coastal and continental air.

GRAPHICAL ABSTRACT

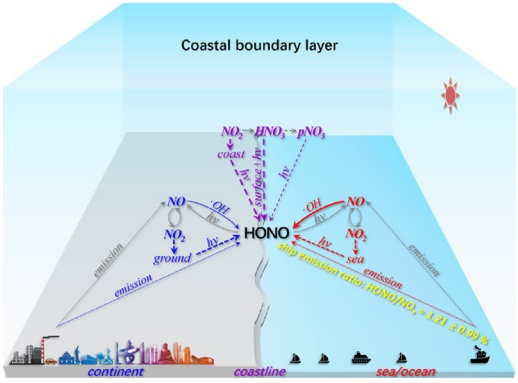

ARTICLE INFO

Article history:
Received 24 December 2021
Received in revised form 1 February 2022
Accepted 1 February 2022
Available online 16 February 2022

Editor: Pingqing Fu

Keywords:
Nitrous acid (HONO)
Ship emission
Budget analysis
Atmospheric oxidising capacity
Coastal boundary layer

ABSTRACT

Nitrous acid (HONO) can significantly contribute to hydroxyl radicals (•OH) and thus regulate atmospheric oxidation chemistry; however, ambient HONO sources are not well quantified and vary in different environments. In this study, we conducted comprehensive field observations at a coastal site in the South China Sea and performed chemical box modelling to demonstrate contrasting budgets and impacts of diurnal atmospheric HONO derived from the sea, coastline and continent. The ship emission ratio of HONO/nitrogen oxides (NO_x) (1.21 ± 0.99%) was calculated from hundreds of night-time fresh plume measurements. Offshore marine air was frequently influenced by ship exhausts, and the sea acted as an HONO sink. Heterogeneous conversions of nitrogen dioxide (NO_2) on underlying surfaces and photolysis of adsorbed nitric acid ($HNO_{3(ads)}$) were the major HONO sources in coastal air, when heterogeneous NO_2 conversions on the ground surface and the homogeneous NO + •OH reaction dominated HONO formation in continental air. HONO photolysis was a significant source of reactive radicals (RO_x = •OH + HO_2• + RO_2•) in these air masses. Atmospheric box model including only homogeneous HONO source of the NO + •OH reactions significantly underpredicted the •OH concentration and atmospheric oxidising capacity in coastal and continental air. This study provides new insights into the complex sources and significant impacts of HONO in the polluted coastal boundary layer.

* Corresponding authors.
E-mail addresses: xuelikun@sdu.edu.cn (L. Xue), tao.wang@polyu.edu.hk (T. Wang).

http://dx.doi.org/10.1016/j.scitotenv.2022.153692

1. Introduction

Nitrous acid (HONO) is a significant contributor to the hydroxyl radicals (•OH), which is the most powerful oxidant initiating daytime atmospheric oxidation processes and affecting regional air quality (Gligorovski et al., 2015; Kim et al., 2014; Stutz et al., 2013; Xue et al., 2016). Despite such profound environmental consequences, ambient HONO sources are not well quantified (Wang et al., 2021; Zhang et al., 2021). Known sources of HONO include the homogeneous reaction of nitric oxide (NO) with •OH, heterogeneous conversions of nitrogen dioxide (NO_2) on various surfaces (Ammann et al., 1998; Liu et al., 2020; Liu et al., 2014; Ma et al., 2017; Stemmler et al., 2006; VandenBoer et al., 2013; Yang et al., 2021b), photolysis of particulate nitrate (pNO_3) and surface-adsorbed nitric acid ($HNO_{3(ads)}$) (Romer et al., 2018; Ye et al., 2016a; Ye et al., 2017; Ye et al., 2016b; Zhou et al., 2011), and primary emissions from fuel combustion and soil–air exchange (Liang et al., 2017; Liao et al., 2021; Oswald et al., 2013; Peng et al., 2020; Wang et al., 2021; Wormhoudt et al., 2007; Xue et al., 2021). However, some key parameters and processes of these known HONO generation pathways are highly variable and uncertain (Liu et al., 2019; Xue et al., 2020). In particular, HONO emissions from ship exhausts have received limited attention, despite the rapid development of the global shipping industry and the dense maritime traffic in many coastal areas (United Nations Conference On Trade and Development, 2020; Liu et al., 2016). Recently, the $\Delta HONO/\Delta NO_x$ (where NO_x = nitrogen oxides) emission ratio of a single medium-speed diesel engine vessel during its cruise was calculated to be 0.51 ± 0.18%, and a global ship HONO emission inventory was developed (Sun et al., 2020). Model simulations show that ship-contributed HONO could enhance the concentrations of fine particulate matter ($PM_{2.5}$), ozone (O_3) and reactive radicals (RO_x = •OH + HO_2• + RO_2•, where HO_2•/RO_2• are the hydro/organic peroxy radicals) over the South China Sea by 1%, 6% and 12%, respectively (Dai and Wang, 2021).

Ocean covers approximately 71% of Earth's surface, and over 60% of the global population is concentrated in coastal areas. In the coastal boundary layer, atmospheric compositions and chemical processes differ depending on whether air originates from the sea, coastline or continent (Crowley et al., 2011). Most HONO researches have been dedicated to understanding its sources and impacts in human-perturbed inland areas (Fu et al., 2019; Liu et al., 2021; Liu et al., 2019), whereas few studies have investigated HONO chemistry in marine and coastal atmospheres.

The nocturnal conversion rate of NO_2 to HONO in marine air was found to be significantly larger than that in air from the land, suggesting oceanic HONO production (Yang et al., 2021a; Zha et al., 2014). Wen et al. (2019) proposed that HONO production in the marine boundary layer might result from air–sea interaction and photochemical formation in the sea-surface microlayer, contradicting the previously accepted hypothesis that the sea surface serves as an HONO sink due to its alkaline nature (Beine et al., 2005; Wojtal et al., 2011). A recent airborne study found rapid reactive nitrogen recycling in the marine atmosphere of the North Atlantic Ocean and suggested that pNO_3 photolysis is a significant HONO source in this region (Ye et al., 2016b), in contrast to the NO_x-dominated HONO formation process in polluted continental areas. Overall, there is incomplete knowledge of marine HONO sources and processes, meaning that investigations are needed on HONO sources in marine air, anthropogenic activities and marine atmospheric processes interactions, and their impacts on coastal air quality.

Hong Kong lies adjacent to the South China Sea and the Northwest Pacific Ocean and is located in the southeast of the Guangdong–Hongkong–Macao Greater Bay Area, one of the world's largest urban agglomerations (Fig. 1). Driven by the Asian monsoon and sea–land breezes, Hong Kong receives air masses from multiple sources, including relatively clean marine air, polluted air masses derived from ship exhausts from surrounding navigation waters, and transported continental air (Wang et al., 2009). Therefore, Hong Kong is a suitable location to study HONO chemistry in dissimilar air masses derived from different environments. We therefore conducted intensive field experiments at a site on the southeast coast of Hong Kong in 2018, measuring a suite of chemical and meteorological parameters. These data facilitated a comprehensive HONO source analysis in four distinct air masses (ship exhausts, marine, coastal and continental air masses) and detailed modelling of the impacts of HONO chemistry on atmospheric oxidising capacity (AOC). Our findings enrich understanding of the complex sources and significant impacts of HONO in the coastal boundary layer and support the development of a refined inventory of HONO emissions from ships.

2. Methodology

2.1. Field measurements

We conducted field measurements at the Cape D'Aguilar Supersite Air Quality Monitoring Station (22°13′N, 114°15′E), which is managed by the Hong Kong Environmental Protection Department. This typical coastal background station sits on the southeastern tip of Hong Kong island and is 60 m above sea level (see Fig. 1), a site that receives a variety of air masses, including marine air, continental air and ship plumes (Wang et al., 1998; Wang et al., 2009). Two intensive observation campaigns

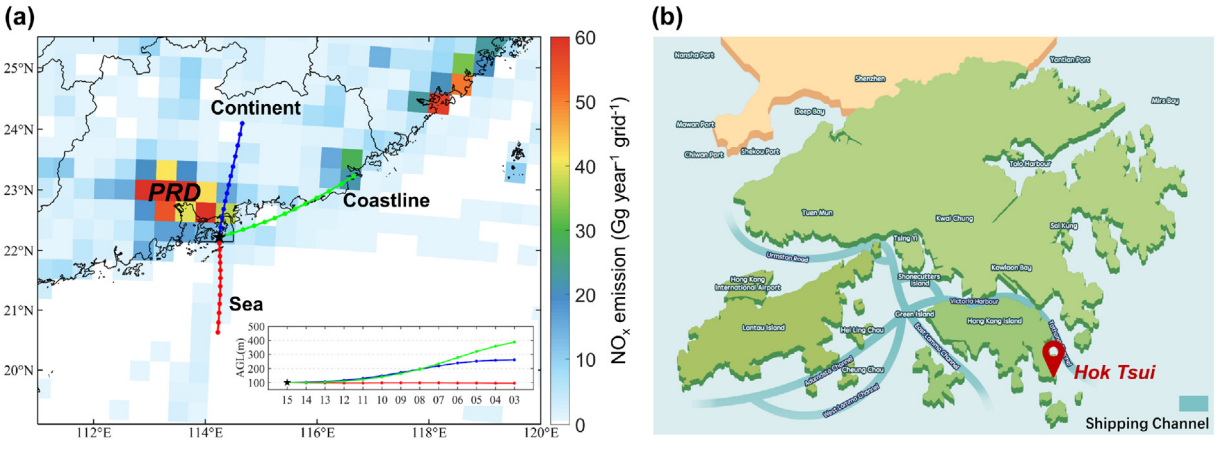

Fig. 1. Maps showing the study area and observation site. (a) Position of the measurement site in the Guangdong–Hongkong–Macao Greater Bay Area, and the 12-h backward trajectory clusters of air masses coming from three typical coastal environments of the sea, coastline and continent. The map is color-coded with anthropogenic NO_x emission intensity. (b) Location of the measurement site of Hok Tsui and the major shipping channels in Hong Kong. Anthropogenic NO_x emission data in grids of 27 km × 27 km are obtained from the MEIC (2017) (http://meicmodel.org/, last access 26 February) for mainland China (Liu and Wang, 2020), the MIX (2010) for Hong Kong, and the HTAP (2010) for the ocean area (Janssens-Maenhout et al., 2015).

were conducted from 31 August to 8 October 2018 and from 31 October to 12 December 2018. Online measurements included HONO and related trace gases (e.g., NO, NO_2, total reactive oxidised nitrogen (NO_y), O_3, carbon monoxide (CO), and sulfur dioxide (SO_2)), 1-, 2.5- and 10-μm particulate matters (PM_1, $PM_{2.5}$ and PM_{10}), water-soluble inorganic ions in $PM_{2.5}$ and PM_{10}, volatile organic compounds (VOCs), aerosol surface area density (S_a) and meteorological parameters (e.g., solar radiation, temperature, relative humidity (RH), wind direction and wind speed).

HONO was measured using a custom-built iodide-anion chemical-ionization mass spectrometer (CIMS; THS Instruments Inc., Atlanta) that was optimised to measure HONO (Wang et al., 2016; Wang, 2020). Briefly, HONO was ionised and combined with iodide anion to form iodide–HONO clusters ($IHONO^-$) and detected by a quadrupole mass spectrometer. During one measurement period (31 August–4 September 2018), we simultaneously measured HONO using the CIMS and a long-path absorption photometer (LOPAP-03; QUMA, Germany), a widely used commercial instrument. Two sets of measured HONO data agreed well, with a correlation coefficient (r^2) of 0.75 (Fig. S1). Detailed description of the HONO measurement using CIMS is provided in Text S1 in the Supplementary Information (SI). The other species and parameters were measured using commercial instruments; detailed measurement information is documented in Table S1.

2.2. Chemical box model simulation

We used a chemical box model equipped with the Master Chemical Mechanisms (MCM, version 3.3.1) to quantify the roles of HONO in atmospheric radical productions and AOC. The MCM box model comprises almost explicit gaseous chemical mechanisms and has been widely used in previous researches (Jiang et al., 2020; Xue et al., 2016). The model was constrained by observational data (concentrations of CO, SO_2, O_3, NO, NO_2, VOCs, and meteorological parameters) averaged at 10-min time intervals for all but VOCs, which were collected at 1-h intervals. Before each formal simulation, we conducted a three-day spin-up constrained by observational data to reach stable states for the unconstrained species. In each case, two runs with/without measured HONO constraint were conducted to reveal the impacts of HONO sources besides the NO + •OH reaction on atmospheric oxidation chemistry. The model configuration details are provided in Text S2.

3. Results and discussion

3.1. Overview of observation data

Timeseries of the atmospheric trace compositions and meteorological conditions measured at the site are presented in Fig. S2 (10-min data-point intervals, except 1-h data-point intervals for HNO_3 and pNO_3). Overall, the observation results revealed highly variable moderate air pollution. The 10-min mean ± standard deviation (SD) concentration of HONO was 0.18 ± 0.15 ppbv. This is significantly lower than those at suburban coastal sites in eastern and southern China and a strait in Canada (Cui et al., 2019; Wojtal et al., 2011; Xu et al., 2015; Yang et al., 2021a), comparable to that in the inland Bohai Sea in northern China (Wen et al., 2019), 50% higher than that measured 6 years ago at a site near the present station (Zha et al., 2014), and substantially higher than those in more remote marine boundary layers in the North Atlantic Ocean and the Mediterranean Sea (Meusel et al., 2016; Ye et al., 2016b). This intermediate concentration of HONO is consistent with the moderate concentrations of its precursors, such as NO (0.66 ± 1.83 ppbv), NO_2 (4.28 ± 4.38 ppbv), HNO_3 (0.25 ± 0.12 ppbv) and pNO_3 (3.3 ± 1.7 μg m^{-3}, concentration in PM_{10}).

3.2. Ship emission of HONO

3.2.1. Ship plumes selection

The timeseries (Fig. S2) show frequent short-term concentration spikes of SO_2 and NO_x, indicating impacts from ship plumes from the dense maritime traffic in Hong Kong's waters and the surrounding waters (Wang et al., 2003). To examine the emission ratios of HONO in ship exhausts, we adopted a set of criteria to screen out ship plumes (Table S2). First, only data within the highest 25% of NO_x and SO_2 concentrations were considered. Second, data with short-term (<2 h) SO_2 concentration spikes were identified as ship plumes (SPs), and those with NO_x/NO_y ratios ≥90% were considered fresh ship plumes (FSPs). Eventually, we selected data from 567 SPs and 272 FSPs based on these criteria. Fig. 2a shows representative examples of identified SPs, and Fig. S2 shows all of the SPs observed in this study. Data within the lowest 5% of NO_x and $PM_{2.5}$ concentrations were considered background air characteristics, and 13 background cases (BGCs) were identified and used to remove the influence of background concentrations from calculations of ship emission ratios (see next section). Table S3 and Fig. 4 show statistics of the measured species and parameters in the ship plumes and BGCs. HONO concentrations were lowest in the BGCs (0.01 ± 0.01 ppbv), higher in FSPs (0.17 ± 0.21 ppbv) and highest in SPs (0.23 ± 0.22 ppbv), with corresponding $HONO/NO_x$ ratios of 0.012 ± 0.016, 0.011 ± 0.009 and 0.022 ± 0.021, respectively. These notably enhanced HONO concentrations in FSPs and SPs compared to BGCs indicate that ships release high concentrations of HONO. The higher HONO concentrations and $HONO/NO_x$ ratios in SPs than in FSPs suggest there is considerable HONO production during the ageing of FSPs.

3.2.2. Ship emission ratio of $HONO/NO_x$

The $HONO/NO_x$ emission ratio ($ER_{HONO/NOx}$) is a key parameter for evaluating the characteristics and intensity of HONO emission from ships. $ER_{HONO/NOx}$ was deduced in this study using Eq. (1).

$$HONO/NO_x = \frac{HONO_{(FSP)} - HONO_{(BGC)}}{NO_{x\,(FSP)} - NO_{x(BGC)}} \quad (1)$$

where $HONO_{(FSP)}$ and $NO_{x(FSP)}$ are the HONO and NO_x concentrations in FSPs, and $HONO_{(BGC)}$ and $NO_{x(BGC)}$ are the average HONO and NO_x concentrations in BGCs, respectively. To negate the influence of light on HONO chemistry, only night-time FSPs (n = 151) were included in the $ER_{HONO/NOx}$ calculation. The ship $ER_{HONO/NOx}$ varied from 0.21% to 5.30% (75% within 0.20–1.40% and 25% > 1.40%) with a mean ± SD of 1.21 ± 0.99% and a median of 0.91% (Fig. 2b). This large variation in ship $ER_{HONO/NOx}$ is similar to that of vehicles and is due to the diversity of engine types, fuels, operation conditions and other factors (Kurtenbach et al., 2001; Liang et al., 2017; Nakashima and Kajii, 2017). As shown in Fig. 2b, the $ER_{HONO/NOx}$ obtained in this study is more than double and more variable than that reported by Sun et al. (2020) (mean ± SD, 0.51 ± 0.18%; median, 0.43%; 90% within 0.08–0.97%). The emission ratios in Sun et al. (2020) were derived from only one small vessel (with a gross tonnage of 3235 tons) equipped with a medium-speed engine and fuelled by high-quality light marine diesel oil. In contrast, the present study was conducted near a navigation area in one of the world's busiest harbour cities. The diversity of vessels and complexity of ambient conditions in the study area accounts for the much higher and broader ship $ER_{HONO/NOx}$ than that of Sun et al. (2020).

3.2.3. Ship plumes ageing process

The $HONO/NO_x$ ratio as a function of $-\log_{10}(NO_x/NO_y)$, an indicator of photochemical age (Kleinman et al., 2008; Nie et al., 2012), is illustrated in a scatter plot in Fig. 2c. As ship plumes age, their $HONO/NO_x$ ratio gradually increases. For example, as $-\log_{10}(NO_x/NO_y)$ increased from 0.05 to 0.30, the NO_x/NO_y ratio decreased from 0.90 to 0.50, and the average $HONO/NO_x$ proportion rose from 1.64% to 5.79%, tripling from 1.54% to 4.57% in the daytime and quadrupling from 1.78% to 7.15% at night. These rising trends show that there is HONO formation during ship plume ageing, confirming that ship emissions are a significant source of HONO in coastal and maritime areas with abundant shipping traffic.

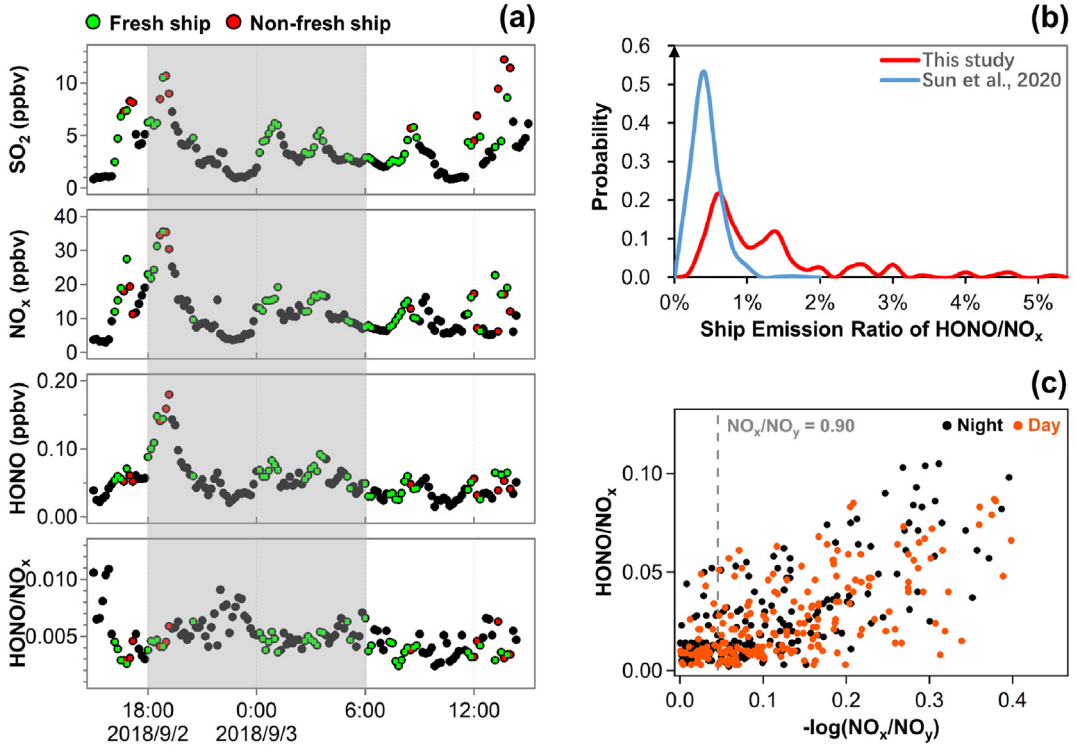

Fig. 2. Ship emission of HONO. (a) Examples of ship plumes in the time series of SO_2, NO_x, HONO and HONO/NO_x. Grey shaded area marks the night period. (b) Probability histograms of the ship emission ratio of HONO/NO_x in this study and Sun et al. (2020). (c) The ratio of HONO/NO_x against the ageing process of all ship plumes during the day and night.

3.3. Contrasting characteristics, chemical budgets and impacts of HONO in marine, coastal and continental air masses

3.3.1. Selection of different air masses

Three types of air masses – originating from the sea, coastline and continent – were selected by examining backward trajectory and wind information. Within the 24 h of a day, when all 12-h backward trajectories (computed hourly using the HYSPLIT model) and the average wind were both from the sea (or coastline, continent) (Stein et al., 2015), the day was regarded as a marine (or coastal, continental) air-dominated case. With such strict criteria, 4, 11 and 7 days were classified as marine, coastal and continental air cases, respectively (see Fig. 1 for the three types of trajectory clusters and Fig. S2 for the individual cases). Air masses from the sea were frequently influenced by ship plumes, as indicated by their spikes in SO_2 and NO_x concentrations. For this reason, we applied more rigorous screening criteria to the marine air cases: only marine air data within the lowest 50% of SO_2 and NO_x concentrations were selected for further analysis (194 data points).

3.3.2. Air mass characteristics

Fig. 4 shows the average physical and chemical features of the three types of air masses. Marine air was very humid (RH = 93 ± 3%), with the highest freshness (NO_x/NO_y = 0.89 ± 0.19) and lowest air pollutant concentrations. Coastal air was humid (RH = 82 ± 4%), with the highest degree of ageing (NO_x/NO_y = 0.53 ± 0.23) and moderate air pollutant concentrations, except for that of pNO_3, which was the highest in coastal air. Continental air was relatively dry (RH = 63 ± 14%), with a moderate degree of ageing (NO_x/NO_y = 0.75 ± 0.21) and the highest concentrations of air pollutants, especially NO_x. The average HONO concentrations were 0.03 ± 0.01, 0.10 ± 0.05 and 0.32 ± 0.14 ppbv in marine, coastal and continental air, respectively, with respective HONO/NO_x ratios of 0.008 ± 0.003, 0.067 ± 0.054 and 0.074 ± 0.065.

The diurnal variations in HONO and the HONO/NO_x ratio are shown in Fig. 3. The HONO concentration presented a typical diel pattern in continental air, reaching a maximum at approximately midnight and a minimum at noon, whereas concentrations remained relatively stable throughout the day in marine and coastal air. Considering the rapid photolytic loss of

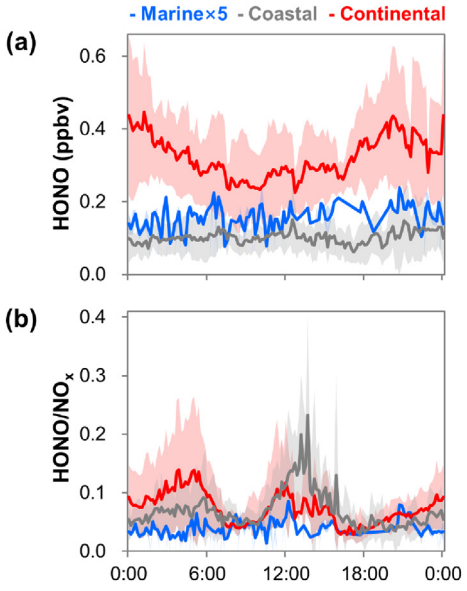

Fig. 3. Averaged diurnal variations of (a) HONO and (b) HONO/NO_x in air masses coming from the sea (Marine), coastline (Coastal) and continent (Continental). Shaded areas show standard deviations (±1σ). Note that the values of HONO and HONO/NO_x in marine air are magnified five time.

HONO in the daytime, especially at noon, the stable HONO concentration throughout the day suggests that HONO is sufficiently emitted and/or generated in marine and coastal air. The HONO/NO_x ratio varied slightly in marine air remaining approximately 0.008, but fluctuated sharply showing two peaks before sunrise and around noon in both coastal (0.092 and 0.232) and continental (0.139 and 0.118) air. While the dawn peak was ascribable to night-time HONO accumulation, the noon peak could be due to enhanced photolytic sources. The HONO/NO_x ratio increased sharply at approximately noon in coastal air, to a level twice that in continental air, suggesting that there was a greater increase in photo-related HONO production in coastal air than in continental air.

3.3.3. HONO budgets

We conducted a HONO budget analysis to explore the contributions of different sources in marine, coastal and continental air (Liu et al., 2021; Oswald et al., 2015; Wang et al., 2017; Xue et al., 2020). We considered HONO derived from on-road vehicular emission, the homogeneous NO + •OH reaction, light-sensitive heterogeneous NO_2 conversion on terrestrial, sea and aerosol surfaces and $HNO_{3(ads)}$ and pNO_3 photolysis, which have been reported as potentially significant HONO contributors. HONO from other sources (e.g., HO_2·H_2O + NO_2 reaction, NO_2^* + H_2O reaction and ortho-nitrophenol photolysis) were not considered because their reaction rate constants were negligible or there were no relevant data available. The HONO sinks included in the analysis were photolysis, the HONO + •OH reaction and dry deposition. More details of the budget analysis method are provided in the SI (Text S3). Note that some parameters (e.g., emission ratios, reaction rate constants and precursor uptake coefficients) used for the budget calculation are subject to uncertainties. We adopted the commonly used values in our analysis and performed sensitivity tests to examine their impacts on the results.

Fig. 5 shows the average daytime (09:00–17:00, local time (LT)) production rates of HONO (P_{HONO}) calculated from individual sources [P_{HONO}(cal)] and deduced from observations [P_{HONO}(obs)], where P_{HONO}(obs) equals the sum of the observed changing rate and total calculated loss rate of HONO. The P_{HONO}(obs) values in marine, coastal and continental air were 0.06 ± 0.01, 0.25 ± 0.08 and 0.82 ± 0.24 ppbv h^{-1}, respectively. Continental air masses pass through the Pearl River Delta urban agglomerations (Fig. 1); thus, their higher P_{HONO}(obs) value reflects the significant effects of human activities on HONO chemistry in the coastal boundary layer of southern China. The budget analysis shows that P_{HONO}(cal) was much higher than P_{HONO}(obs) in marine air but matched the daytime variations of P_{HONO}(obs) in coastal and continental air.

The source contributions to HONO differed between the three air mass types. In marine air (Fig. 5a), the homogeneous NO + •OH reaction (45.8 ± 6.7%) and the heterogeneous NO_2 conversion on the sea surface (39.0 ± 2.9%) dominated daytime HONO formation, both of which far exceeded the P_{HONO}(obs). Note that we have assumed the same NO_2 uptake coefficient and conversion efficiency on the sea surface as on the land surface. The large contributions of NO_x to in-situ HONO production suggest that ship emissions strongly affected the selected marine-air cases. P_{HONO}(cal) was higher than P_{HONO}(obs), implying that compared to other areas, there were larger HONO losses in the marine boundary layer, where more efficient HONO uptake by the alkaline sea may occur.

In coastal air (Fig. 5b), $HNO_{3(ads)}$ and pNO_3 photolysis were the most significant sources of HONO (38.5 ± 3.7% totally) around noon (11:00–14:00 LT), and the heterogeneous NO_2 conversion on the underlying surface governed HONO formation throughout the remainder of the day (40.7 ± 5.4% throughout the daytime). Coastal air featured moderate NO_2 concentrations and abundant secondary pollutants, such as total oxidised nitrogen (TNO_3 = HNO_3 + pNO_3) (Fig. 4). Efficient TNO_3 re-noxification to nitrogen oxides, in which HONO is an intermediate that readily photolyses to NO, could greatly promote the recycling of TNO_3-HONO-NO_x in coastal air.

In continental air (Fig. 5c), NO_x-related sources – the heterogeneous conversion of NO_2 to HONO on the ground surface (54.7 ± 12.2%) and the NO + •OH reaction (25.5 ± 9.7%) – were the major contributors to daytime HONO formation. The contribution of the NO + •OH reaction reached a maximum in the morning (09:00–10:00 LT; 39.2 ± 2.0%), and the heterogeneous conversion of NO_2 on the ground surface showed increasing contributions as the day progressed. $HNO_{3(ads)}$ photolysis (11.0 ± 3.5%) and on-road vehicle emissions (7.4 ± 4.7%) were also significant sources of daytime HONO; the contributions from on-road vehicular emissions reached a peak in the morning and evening and reached a valley at approximately noon, whereas $HNO_{3(ads)}$ photolysis exhibited an opposite daytime trend.

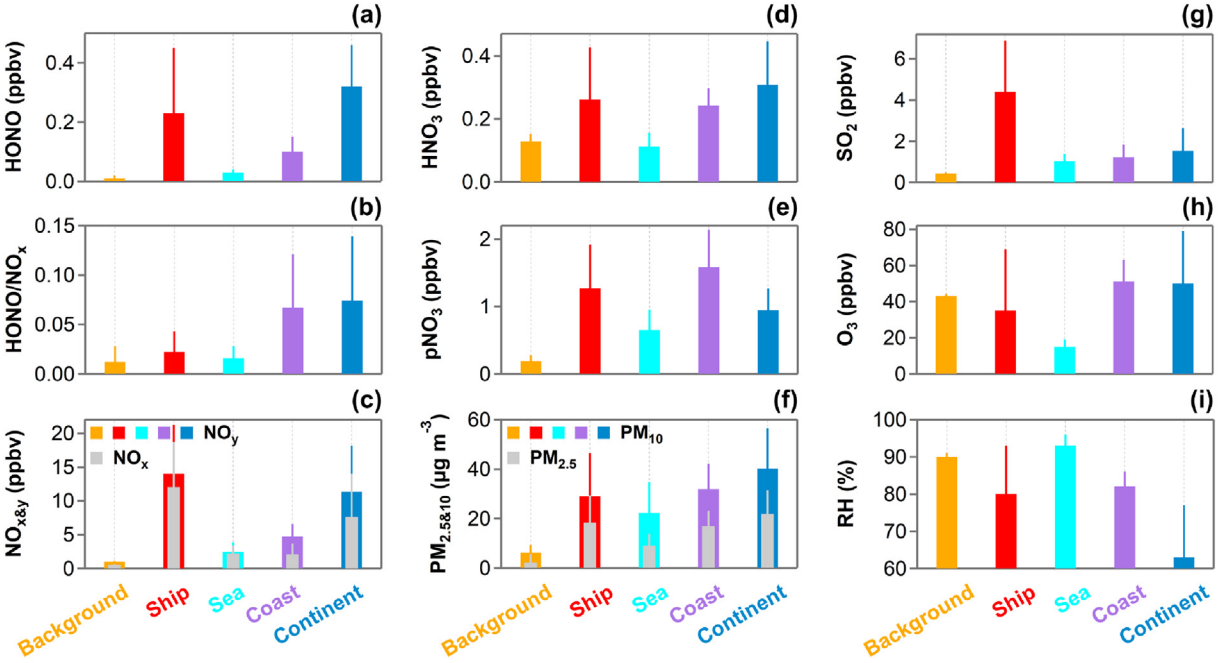

Fig. 4. Atmospheric chemical compositions in different types of plumes. Average concentrations of (a) HONO, (b) HONO/NO_x, (c) $NO_{x\&y}$, (d) HNO_3, (e) pNO_3, (f) $PM_{2.5\&10}$, (g) SO_2, (h) O_3, and (i) RH in the five types of air masses, namely, background, ship, marine, coastal, and continental air. Error bars show the standard deviations (±1σ).

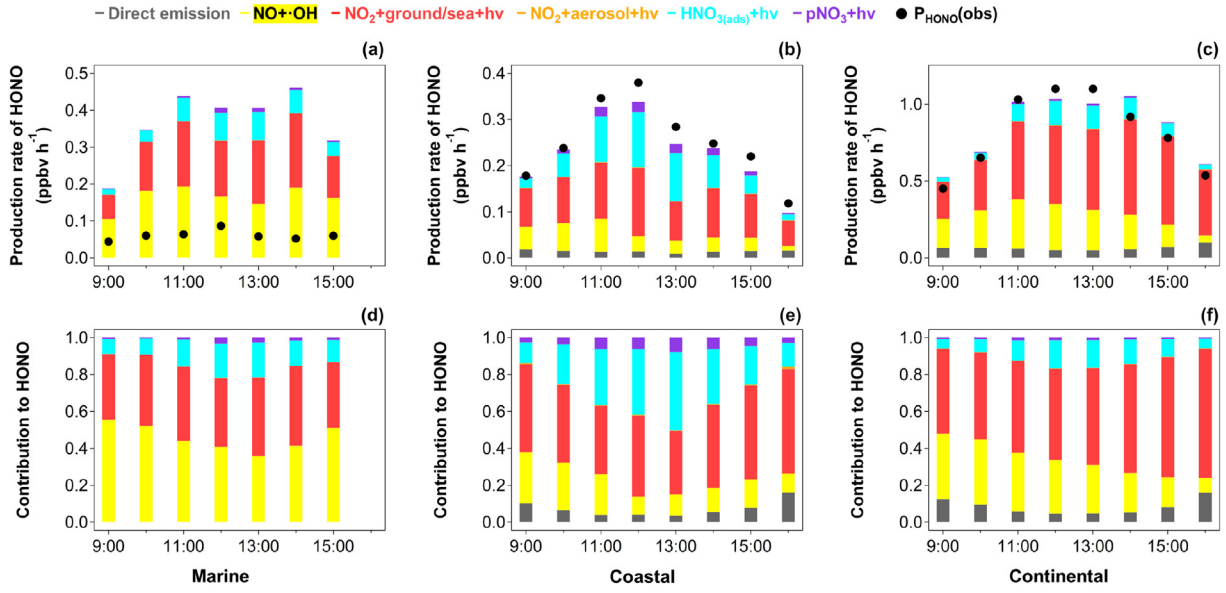

Fig. 5. Average daytime variations in the production rates of HONO calculated from individual sources (bars, upper panel) and deduced from observations and sinks (dots, upper panel) and the contribution of each source (lower panel) in different air masses coming from the sea (left), coastline (middle) and continent (right). P_{HONO}(obs) equals the sum of the observed changing rate and the calculated total loss rate, of HONO.

To assess the uncertainties of the source contributions, we performed sensitivity analyses using both upper and lower values for individual parameters (Table S4), which were the vehicular HONO/NO_x emission ratio ($ER_{HONO/NOx}$), the NO_2 uptake coefficients on various surfaces (γ_{NO2}), and the photolysis frequencies of $HNO_{3(ads)}$ [$j(HNO_{3(ads)})$] and pNO_3 [$j(pNO_3)$]. Fig. 6 shows the average diurnal sensitivity results. Overall, the uncertainties caused by vehicular $ER_{HONO/NOx}$, γ_{NO2} on aerosol surfaces and $j(pNO_3^-)$ were small, mostly because of their low contributions to HONO production at our site. The major uncertainties were detected in the parameterisations of γ_{NO2} on the ground surface and $j(HNO_{3(ads)})$, which were key parameters of the two principal HONO formation pathways here. Adjusting γ_{NO2} on the ground surface led to an HONO production rate far beyond the P_{HONO}(obs) or lower than the P_{HONO}(NO + •OH) in all air types. Similarly, adjusting $j(HNO_{3(ads)})$ produced a HONO production rate far outside the range between P_{HONO}(obs) and P_{HONO}(NO + •OH) in marine and coastal air. However, in continental air, the budget result was not so sensitive to $j(HNO_{3(ads)})$ adjustment because of the limited contribution of $HNO_{3(ads)}$ photolysis to HONO production; the abundant fresh exhausts (e.g., NO_x) indicate the significant roles of on-road emission and NO_2 conversions in HONO production, and the small proportion of secondary pollutants (e.g., HNO_3) suggests the limited contribution of high-oxidation-state nitrogen photolysis to HONO. The sensitivity analysis results suggest there were significant uncertainties in HONO production from individual sources, which implies that our quantifications of HONO sources were also of uncertainty. Thus, more accurate parameterisations of these sources are needed because these parameters are fundamental to achieving a comprehensive understanding of HONO chemistry in various environments.

3.3.4. HONO impacts on AOC

Fig. 7 shows the average daytime variations in the primary production rates of RO_x radicals in the three types of air masses. The daytime

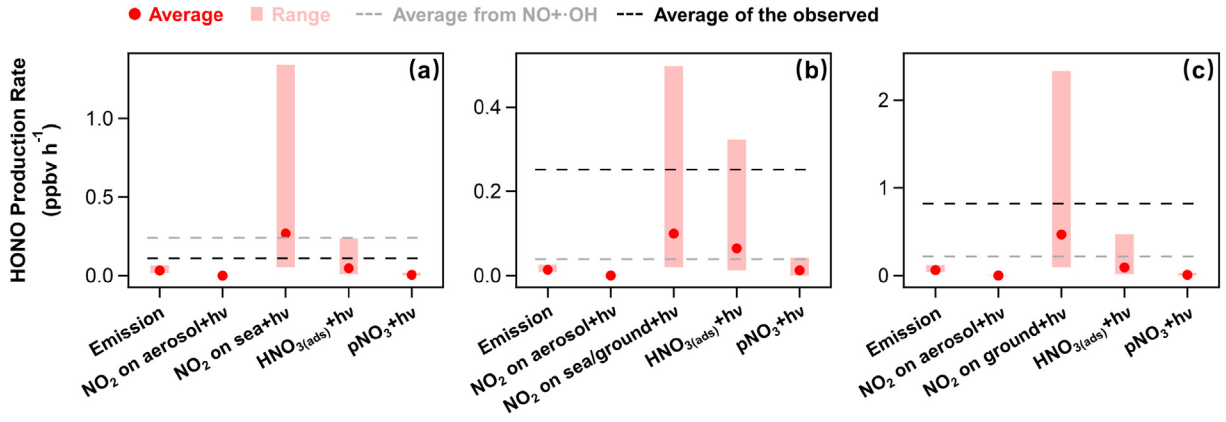

Fig. 6. Sensitivity results of diurnal (09:00–17:00) HONO production rates (P_{HONO}) from different sources in (a) marine, (b) coastal and (c) continental air. The considered HONO sources include direct emission, photo-induced heterogeneous conversion of NO_2 on aerosol/ground (or sea) surfaces, photolysis of adsorbed HNO_3 ($HNO_{3(ads)}$), and photolysis of particulate nitrate (pNO_3). The red dot is the average P_{HONO} from each source, the red column indicates the sensitivity range of P_{HONO} from each source, the black dashed line is the average observed P_{HONO}, and the grey dashed line represents the P_{HONO} from NO + •OH.

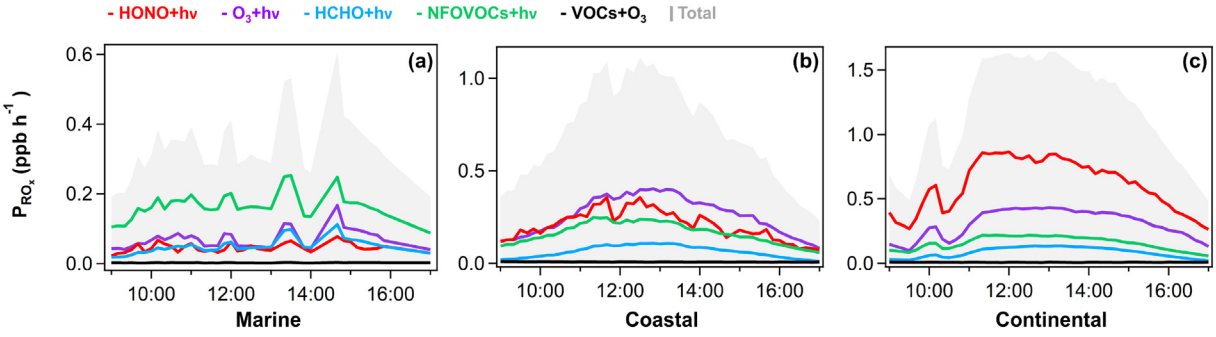

Fig. 7. Average daytime primary production rates of reactive radicals (RO_x = •OH + HO_2• + RO_2•) in air masses coming from the (a) sea, (b) coastline and (c) continent in the coastal boundary layer of the PRD. Here the considered major primary radical sources include photolysis of HONO, O_3, formaldehyde (HCHO), and OVOCs except for HCHO (NFOVOCs), and the reactions of O_3 with unsaturated VOCs.

(09:00–17:00 LT) RO_x production rates were 0.34 ± 0.09, 0.71 ± 0.26 and 1.17 ± 0.39 ppb h^{-1} in marine, coastal and continental air, respectively. In marine air, the photolysis of oxygenated VOCs (OVOCs, including formaldehyde (HCHO)) was the dominant source of radicals (64.7%; 14.9% for HCHO alone), followed by O_3 photolysis (20.6%), HONO photolysis (14.7%) and the negligible ozonolysis reactions of unsaturated VOCs. In coastal air, the predominant sources of radicals were the photolysis of O_3 (36.6%), OVOCs (32.4%; 9.1% for HCHO alone) and HONO (29.6%), and then the reactions of O_3 + VOCs (1.4%). In continental air, the photolysis of HONO was the dominant radical source (52.1%), followed by the photolysis of O_3 (26.5%) and OVOCs (20.5%; 7.3% for HCHO alone) and reactions of O_3 + VOCs (0.9%). RO_x concentrations increased from marine to coastal to continental air (Fig. S3), and the contribution of HONO photolysis to RO_x production followed a similar increasing trend. These results suggest that HONO plays a significant role in atmospheric oxidation in the coastal boundary layer, especially in polluted continental environments.

As the basic MCM model (version 3.3.1) used here only includes homogeneous HONO formation from the NO + •OH reaction, we assessed the magnitudes of •OH radical and AOC underprediction using the default HONO scheme. AOC was defined as the sum of reaction rates between the •OH radical and reduced substances (i.e., CO, CH_4, VOCs, NO, NO_2 and SO_2) (Xue et al., 2016). We conducted two runs with/without the constraint of observed HONO data; the difference between the simulation results represents the contributions of HONO sources except for the NO + •OH reaction. Fig. 8 shows that the model run with only NO + •OH as the HONO source compared well with HONO-constrained simulation for marine air but significantly underestimated the •OH concentrations and AOCs of coastal and continental air. The former can be explained by the underestimation of HONO loss rates in marine air, and the latter by the important role of heterogeneous and photolytic HONO sources in coastal and continental air, as reflected in the budget analysis results. Quantitatively, underestimations by model runs including only NO + •OH reaction were 21.4 ± 2.2% and 24.8 ± 2.1% for the average daytime •OH concentration and AOC in coastal air, respectively, further increasing to 42.4 ± 2.4% and 47.3 ± 2.8% for continental air. The magnitudes of underestimates are comparable to those reported in other studies performed in mountainous and coastal regions (Jiang et al., 2020; Yang et al., 2021a). These results demonstrate that atmospheric chemistry models must incorporate a greater range of HONO sources, especially in simulations of polluted atmospheres.

4. Summary and conclusions

This research reported HONO and relevant chemical constituents and meteorological parameters at a coastal site in southern China during the autumn in 2018. The results provide insights into direct HONO emissions from ships and show significant contrasts in pollution characteristics,

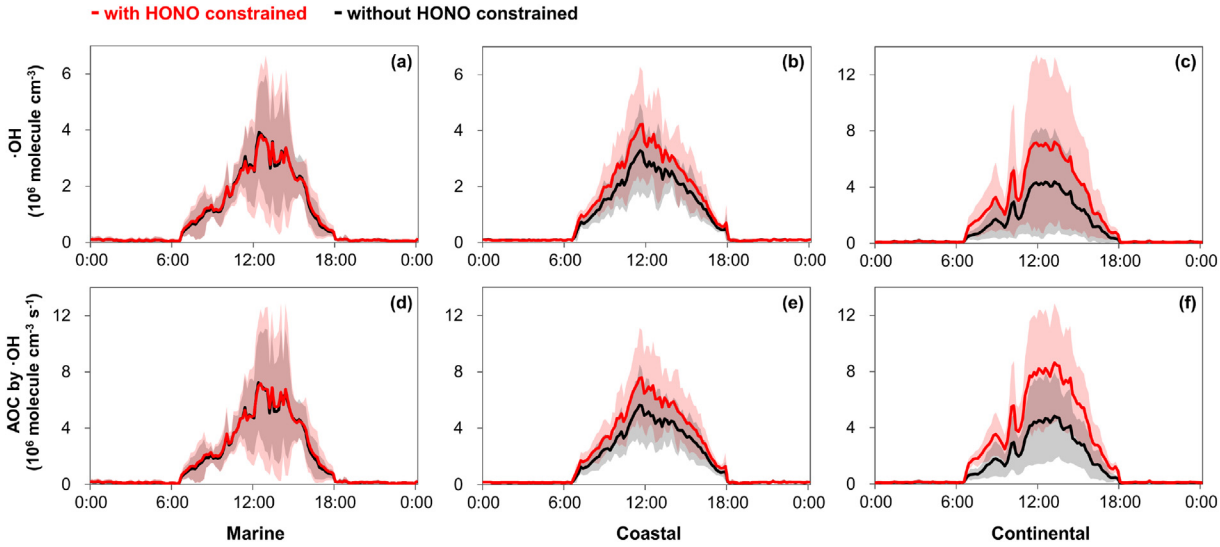

Fig. 8. Comparisons of averaged model-simulated diurnal •OH concentration (upper panel) and atmospheric oxidising capacity (AOC) by •OH (lower panel) between two model runs with/without (red/black) constraints of measured HONO in marine (left), coastal (middle) and continental (right) air. The differences present impacts of HONO sources except for the NO + •OH reaction on the modelling results. Shaded areas mark standard deviations (±1σ).

HONO budgets and radical chemistry in air masses originating from the sea, coastline and continent. An average ship HONO/NO_x emission ratio of 1.21 ± 0.99% was obtained from hundreds of night-time fresh ship plumes. HONO budget calculations suggest that the gas-phase NO + •OH reaction is the dominant HONO source in ship emission-perturbed marine air and that the sea surface likely serves as an HONO sink. Heterogeneous NO_2 conversion on underlying surfaces and surface-adsorbed HNO_3 photolysis were the main sources of HONO in coastal air, and heterogeneous NO_2 conversion on the ground surface as well as homogeneous NO + •OH reaction dominated HONO formation in continental air. HONO photolysis contributed significantly to RO_x radicals in all three types of air, and its contribution to RO_x and AOC increased from marine to coastal to continental air. This study provides new information on HONO sources and impacts in the polluted coastal boundary layers and highlights the necessity of comprehensively considering HONO sources in air quality and climate change modelling.

CRediT authorship contribution statement

Rongrong Gu carried out the data analysis and wrote the manuscript. **Weihao Wang**, **Xiang Peng**, **Men Xia** and **Ya'nan Wang** conducted the field observations and data curation. **Min Zhao** and **Yingnan Zhang** performed the box model simulations. **Yiming Liu** plotted some figure. **Hengqing Shen** participated in the research discussion. **Tao Wang** and **Likun Xue** designed the study and revised the manuscript. **Wenxing Wang** provided resources.

Declaration of competing interest

The authors declare that they have no known competing financial interests or personal relationships that could have appeared to influence the work reported in this paper.

Acknowledgments

The authors are grateful to Steven Poon for assisting the field study, the Hong Kong Environmental Protection Department for providing access to its supersite for us to conduct measurements and for providing data in support of our data analysis, the Hong Kong Observatory for providing measurement data, the Air Resources Laboratory of NOAA for offering the HYSPLIT model, the University of Leeds, National Centre for Atmospheric Science and University of York for providing the Master Chemical Mechanism, and the Tsinghua University for offering the MEIC emission inventory.

Funding

This study was supported by the Hong Kong Research Grants Council (A-PolyU502/16 and T24-504/17-N), the National Natural Science Foundation of China (41922051, 91844301, 42061160478) and the Shandong Provincial Natural Science Foundation for Distinguished Young Scholars (ZR2019JQ09).

Appendix A. Supplementary data

Supplementary data to this article can be found online at https://doi.org/10.1016/j.scitotenv.2022.153692.

References

Ammann, M., Kalberer, M., Jost, D.T., Tobler, L., Rössler, E., Piguet, D., Gäggeler, H.W., Baltensperger, U., 1998. Heterogeneous production of nitrous acid on soot in polluted air masses. Nature 395, 157–160. https://doi.org/10.1038/25965.

Beine, H.J., Amoroso, A., Esposito, G., Sparapani, R., Ianniello, A., Georgiadis, T., Nardino, M., Bonasoni, P., Cristofanelli, P., Dominé, F., 2005. Deposition of atmospheric nitrous acid on alkaline snow surfaces. Geophys. Res. Lett. 32. https://doi.org/10.1029/2005GL022589.

Crowley, J.N., Thieser, J., Tang, M.J., Schuster, G., Bozem, H., Beygi, Z.H., Fischer, H., Diesch, J.M., Drewnick, F., Borrmann, S., Song, W., Yassaa, N., Williams, J., Pöhler, D., Platt, U., Lelieveld, J., 2011. Variable lifetimes and loss mechanisms for NO3 and N2O5 during the DOMINO campaign: contrasts between marine, urban and continental air. Atmos. Chem. Phys. 11, 10853–10870. https://doi.org/10.5194/acp-11-10853-2011.

Cui, L., Li, R., Fu, H., Li, Q., Zhang, L., George, C., Chen, J., 2019. Formation features of nitrous acid in the offshore area of the East China Sea. Sci. Total Environ. 682, 138–150. https://doi.org/10.1016/j.scitotenv.2019.05.004.

Dai, J., Wang, T., 2021. Impact of international shipping emissions on ozone and PM2.5 in East Asia during summer: the important role of HONO and ClNO2. Atmos. Chem. Phys. 21, 8747–8759. https://doi.org/10.5194/acp-21-8747-2021.

Fu, X., Wang, T., Zhang, L., Li, Q., Wang, Z., Xia, M., Yun, H., Wang, W., Yu, C., Yue, D., Zhou, Y., Zheng, J., Han, R., 2019. The significant contribution of HONO to secondary pollutants during a severe winter pollution event in southern China. Atmos. Chem. Phys. 19, 1–14. https://doi.org/10.5194/acp-19-1-2019.

Gligorovski, S., Strekowski, R., Barbati, S., Vione, D., 2015. Environmental implications of hydroxyl radicals (*OH). Chem. Rev. 115, 13051–13092. https://doi.org/10.1021/cr500310b.

Janssens-Maenhout, G., Crippa, M., Guizzardi, D., Dentener, F., Muntean, M., Pouliot, G., Keating, T., Zhang, Q., Kurokawa, J., Wankmüller, R., Denier van der Gon, H., Kuenen, J.J.P., Klimont, Z., Frost, G., Darras, S., Koffi, B., Li, M., 2015. HTAP_v2.2: a mosaic of regional and global emission grid maps for 2008 and 2010 to study hemispheric transport of air pollution. Atmos. Chem. Phys. 15, 11411–11432. https://doi.org/10.5194/acp-15-11411-2015.

Jiang, Y., Xue, L., Gu, R., Jia, M., Zhang, Y., Wen, L., Zheng, P., Chen, T., Li, H., Shan, Y., Zhao, Y., Guo, Z., Bi, Y., Liu, H., Ding, A., Zhang, Q., Wang, W., 2020. Sources of nitrous acid (HONO) in the upper boundary layer and lower free troposphere of the North China Plain: insights from the mount tai observatory. Atmos. Chem. Phys. 20, 12115–12131. https://doi.org/10.5194/acp-20-12115-2020.

Kim, S., VandenBoer, T.C., Young, C.J., Riedel, T.P., Thornton, J.A., Swarthout, B., Sive, B., Lerner, B., Gilman, J.B., Warneke, C., Roberts, J.M., Guenther, A., Wagner, N.L., Dube, W.P., Williams, E., Brown, S.S., 2014. The primary and recycling sources of OH during the NACHTT-2011 campaign: HONO as an important OH primary source in the wintertime. J. Geophys. Res.Atmos. 119, 6886–6896. https://doi.org/10.1002/2013jd019784.

Kleinman, L.I., Springston, S.R., Daum, P.H., Lee, Y.N., Nunnermacker, L.J., Senum, G.I., Wang, J., Weinstein-Lloyd, J., Alexander, M.L., Hubbe, J., Ortega, J., Canagaratna, M.R., Jayne, J., 2008. The time evolution of aerosol composition over the Mexico City plateau. Atmos. Chem. Phys. 8, 1559–1575. https://doi.org/10.5194/acp-8-1559-2008.

Kurtenbach, R., Becker, K.H., Gomes, J.A.G., Kleffmann, J., Lörzer, J.C., Spittler, M., Wiesen, P., Ackermann, R., Geyer, A., Platt, U., 2001. Investigations of emissions and heterogeneous formation of HONO in a road traffic tunnel. Atmos. Environ. 35, 3385–3394. https://doi.org/10.1016/S1352-2310(01)00138-8.

Liang, Y., Zha, Q., Wang, W., Cui, L., Lui, K.H., Ho, K.F., Wang, Z., Lee, S.-C., Wang, T., 2017. Revisiting nitrous acid (HONO) emission from on-road vehicles: a tunnel study with a mixed fleet. J. Air Waste Manag. Assoc. 67, 797–805. https://doi.org/10.1080/10962247.2017.1293573.

Liao, S., Zhang, J., Yu, F., Zhu, M., Liu, J., Ou, J., Dong, H., Sha, Q., Zhong, Z., Xie, Y., Luo, H., Zhang, L., Zheng, J., 2021. High gaseous nitrous acid (HONO) emissions from light-duty diesel vehicles. Environ. Sci. Technol. 55, 200–208. https://doi.org/10.1021/acs.est.0c05599.

Liu, Y., Wang, T., 2020. Worsening urban ozone pollution in China from 2013 to 2017 – part 1: the complex and varying roles of meteorology. Atmos. Chem. Phys. 20, 6305–6321. https://doi.org/10.5194/acp-20-6305-2020.

Liu, Z., Wang, Y., Costabile, F., Amoroso, A., Zhao, C., Huey, L.G., Stickel, R., Liao, J., Zhu, T., 2014. Evidence of aerosols as a media for rapid daytime HONO production over China. Environ. Sci. Technol. 48, 14386–14391. https://doi.org/10.1021/es504163z.

Liu, H., Fu, M., Jin, X., Shang, Y., Shindell, D., Faluvegi, G., Shindell, C., He, K., 2016. Health and climate impacts of ocean-going vessels in East Asia. Nat. Clim. Chang. 6, 1037–1041. https://doi.org/10.1038/nclimate3083.

Liu, Y., Lu, K., Li, X., Dong, H., Tan, Z., Wang, H., Zou, Q., Wu, Y., Zeng, L., Hu, M., Min, K.-E., Kecorius, S., Wiedensohler, A., Zhang, Y., 2019. A comprehensive model test of the HONO sources constrained to field measurements at rural North China Plain. Environ. Sci. Technol. 53, 3517–3525. https://doi.org/10.1021/acs.est.8b06367.

Liu, J., Deng, H., Li, S., Jiang, H., Mekic, M., Zhou, W., Wang, Y., Loisel, G., Wang, X., Gligorovski, S., 2020. Light-enhanced heterogeneous conversion of NO2 to HONO on solid films consisting of fluorene and fluorene/Na2SO4: an impact on urban and indoor atmosphere. Environ. Sci. Technol. 54, 11079–11086. https://doi.org/10.1021/acs.est.0c02627.

Liu, J., Liu, Z., Ma, Z., Yang, S., Yao, D., Zhao, S., Hu, B., Tang, G., Sun, J., Cheng, M., Xu, Z., Wang, Y., 2021. Detailed budget analysis of HONO in Beijing, China: implication on atmosphere oxidation capacity in polluted megacity. Atmos. Environ. 244. https://doi.org/10.1016/j.atmosenv.2020.117957.

Ma, Q., Wang, T., Liu, C., He, H., Wang, Z., Wang, W., Liang, Y., 2017. SO2 initiates the efficient conversion of NO2 to HONO on MgO surface. Environ. Sci. Technol. 51, 3767–3775. https://doi.org/10.1021/acs.est.6b05724.

Meusel, H., Kuhn, U., Reiffs, A., Mallik, C., Harder, H., Martinez, M., Schuladen, J., Bohn, B., Parchatka, U., Crowley, J.N., Fischer, H., Tomsche, L., Novelli, A., Hoffmann, T., Janssen, R.H.H., Hartogensis, O., Pikridas, M., Vrekoussis, M., Bourtsoukidis, E., Weber, B., Lelieveld, J., Williams, J., Pöschl, U., Cheng, Y., Su, H., 2016. Daytime formation of nitrous acid at a coastal remote site in Cyprus indicating a common ground source of atmospheric HONO and NO. Atmos. Chem. Phys. 16, 14475–14493. https://doi.org/10.5194/acp-16-14475-2016.

Nakashima, Y., Kajii, Y., 2017. Determination of nitrous acid emission factors from a gasoline vehicle using a chassis dynamometer combined with incoherent broadband cavity-

enhanced absorption spectroscopy. Sci. Total Environ. 575, 287–293. https://doi.org/10.1016/j.scitotenv.2016.10.050.
Nie, W., Wang, T., Xue, L.K., Ding, A.J., Wang, X.F., Gao, X.M., Xu, Z., Yu, Y.C., Yuan, C., Zhou, Z.S., Gao, R., Liu, X.H., Wang, Y., Fan, S.J., Poon, S., Zhang, Q.Z., Wang, W.X., 2012. Asian dust storm observed at a rural mountain site in southern China: chemical evolution and heterogeneous photochemistry. Atmos. Chem. Phys. 12, 11985–11995. https://doi.org/10.5194/acp-12-11985-2012.
Oswald, R., Behrendt, T., Ermel, M., Wu, D., Su, H., Cheng, Y., Breuninger, C., Moravek, A., Mougin, E., Delon, C., Loubet, B., Pommerening-Roeser, A., Soergel, M., Poeschl, U., Hoffmann, T., Andreae, M.O., Meixner, F.X., Trebs, I., 2013. HONO emissions from soil bacteria as a major source of atmospheric reactive nitrogen. Science 341, 1233–1235. https://doi.org/10.1126/science.1242266.
Oswald, R., Ermel, M., Hens, K., Novelli, A., Ouwersloot, H.G., Paasonen, P., Petäjä, T., Sipilä, M., Keronen, P., Bäck, J., Königstedt, R., Hosaynali Beygi, Z., Fischer, H., Bohn, B., Kubistin, D., Harder, H., Martinez, M., Williams, J., Hoffmann, T., Trebs, I., Sörgel, M., 2015. A comparison of HONO budgets for two measurement heights at a field station within the boreal forest in Finland. Atmos. Chem. Phys. 15, 799–813. https://doi.org/10.5194/acp-15-799-2015.
Peng, Q., Palm, B.B., Melander, K.E., Lee, B.H., Hall, S.R., Ullmann, K., Campos, T., Weinheimer, A.J., Apel, E.C., Hornbrook, R.S., Hills, A.J., Montzka, D.D., Flocke, F., Hu, L., Permar, W., Wielgasz, C., Lindaas, J., Pollack, I.B., Fischer, E.V., Bertram, T.H., Thornton, J.A., 2020. HONO emissions from western US wildfires provide dominant radical source in fresh wildfire smoke. Environ. Sci. Technol. 54, 5954–5963. https://doi.org/10.1021/acs.est.0c00126.
Romer, P.S., Wooldridge, P.J., Crounse, J.D., Kim, M.J., Wennberg, P.O., Dibb, J.E., Scheuer, E., Blake, D.R., Meinardi, S., Brosius, A.L., Thames, A.B., Miller, D.O., Brune, W.H., Hall, S.R., Ryerson, T.B., Cohen, R.C., 2018. Constraints on aerosol nitrate photolysis as a potential source of HONO and NOx. Environ. Sci. Technol. 52, 13738–13746. https://doi.org/10.1021/acs.est.8b03861.
Stein, A.F., Draxler, R.R., Rolph, G.D., Stunder, B.J.B., Cohen, M.D., Ngan, F., 2015. Noaa's hysplit atmospheric transport and dispersion modeling system. Bull. Am. Meteorol. Soc. 96, 2059–2077. https://doi.org/10.1175/BAMS-D-14-00110.1.
Stemmler, K., Ammann, M., Donders, C., Kleffmann, J., George, C., 2006. Photosensitized reduction of nitrogen dioxide on humic acid as a source of nitrous acid. Nature 440, 195–198. https://doi.org/10.1038/nature04603.
Stutz, J., Wong, K.W., Tsai, C., 2013. Disposal of dangerous chemicals in urban areas and mega cities. https://doi.org/10.1007/978-94-007-5034-0_1.
Sun, L., Chen, T., Jiang, Y., Zhou, Y., Sheng, L., Lin, J., Li, J., Dong, C., Wang, C., Wang, X., Zhang, Q., Wang, W., Xue, L., 2020. Ship emission of nitrous acid (HONO) and its impacts on the marine atmospheric oxidation chemistry. Sci. Total Environ. 735. https://doi.org/10.1016/j.scitotenv.2020.139355.
United Nations Conference On Trade and Development, 2020. Review of maritime transport 2020. https://unctad.org/webflyer/review-maritime-transport-2020.
VandenBoer, T.C., Brown, S.S., Murphy, J.G., Keene, W.C., Young, C.J., Pszenny, A.A.P., Kim, S., Warneke, C., de Gouw, J.A., Maben, J.R., Wagner, N.L., Riedel, T.P., Thornton, J.A., Wolfe, D.E., Dubé, W.P., Öztürk, F., Brock, C.A., Grossberg, N., Lefer, B., Lerner, B., Middlebrook, A.M., Roberts, J.M., 2013. Understanding the role of the ground surface in HONO vertical structure: high resolution vertical profiles during NACHTT-11. J. Geophys. Res. Atmos. 118, 10,155–110,171. https://doi.org/10.1002/jgrd.50721.
Wang, W.H., 2020. Investigations of the atmospheric oxidative capacity with chemical ionization mass spectrometry and chemical box model. https://theses.lib.polyu.edu.hk/handle/200/11055 Thesis.
Wang, T., Lam, K.S., Lee, A.S.Y., Pang, S.W., Tsui, W.S., 1998. Meteorological and chemical characteristics of the photochemical ozone episodes observed at Cape D'Aguilar in Hong Kong. J. Appl. Meteorol. 37, 1167–1178. https://doi.org/10.1175/1520-0450(1998)037<1167:maccot>2.0.co;2.
Wang, T., Ding, A.J., Blake, D.R., Zahorowski, W., Poon, C.N., Li, Y.S., 2003. Chemical characterization of the boundary layer outflow of air pollution to Hong Kong during February-April 2001. J. Geophys. Res. Atmos. 108, GTE 8–1-GTE 8-15. https://doi.org/10.1029/2002jd003272.
Wang, T., Wei, X.L., Ding, A.J., Poon, C.N., Lam, K.S., Li, Y.S., Chan, L.Y., Anson, M., 2009. Increasing surface ozone concentrations in the background atmosphere of southern China, 1994–2007. Atmos. Chem. Phys. 9, 6217–6227. https://doi.org/10.5194/acp-9-6217-2009.
Wang, T., Tham, Y.J., Xue, L., Li, Q., Zha, Q., Wang, Z., Poon, S.C.N., Dubé, W.P., Blake, D.R., Louie, P.K.K., Luk, C.W.Y., Tsui, W., Brown, S.S., 2016. Observations of nitryl chloride and modeling its source and effect on ozone in the planetary boundary layer of southern China. J.Geophys.Res.Atmos. 121, 2476–2489. https://doi.org/10.1002/2015JD024556.
Wang, J., Zhang, X., Guo, J., Wang, Z., Zhang, M., 2017. Observation of nitrous acid (HONO) in Beijing, China: seasonal variation, nocturnal formation and daytime budget. Sci. Total Environ. 587–588, 350–359. https://doi.org/10.1016/j.scitotenv.2017.02.159.
Wang, Y., Fu, X., Wu, D., Wang, M., Lu, K., Mu, Y., Liu, Z., Zhang, Y., Wang, T., 2021. Agricultural fertilization aggravates air pollution by stimulating soil nitrous acid emissions at high soil moisture. Environ. Sci. Technol. https://doi.org/10.1021/acs.est.1c04134.
Wen, L., Chen, T., Zheng, P., Wu, L., Wang, X., Mellouki, A., Xue, L., Wang, W., 2019. Nitrous acid in marine boundary layer over eastern Bohai Sea, China: characteristics, sources, and implications. Sci. Total Environ. 670, 282–291. https://doi.org/10.1016/j.scitotenv.2019.03.225.
Wojtal, P., Halla, J.D., McLaren, R., 2011. Pseudo steady states of HONO measured in the nocturnal marine boundary layer: a conceptual model for HONO formation on aqueous surfaces. Atmos. Chem. Phys. 11, 3243–3261. https://doi.org/10.5194/acp-11-3243-2011.
Wormhoudt, J., Herndon, S.C., Yelvington, P.E., Miake-Lye, R.C., Wey, C., 2007. Nitrogen oxide (NO/NO2/HONO) emissions measurements in aircraft exhausts. J. Propuls. Power 23, 906–911. https://doi.org/10.2514/1.23461.
Xu, Z., Wang, T., Wu, J., Xue, L., Chan, J., Zha, Q., Zhou, S., Louie, P.K.K., Luk, C.W.Y., 2015. Nitrous acid (HONO) in a polluted subtropical atmosphere: seasonal variability, direct vehicle emissions and heterogeneous production at ground surface. Atmos. Environ. 106, 100–109. https://doi.org/10.1016/j.atmosenv.2015.01.061.
Xue, L., Gu, R., Wang, T., Wang, X., Saunders, S., Blake, D., Louie, P.K.K., Luk, C.W.Y., Simpson, I., Xu, Z., Wang, Z., Gao, Y., Lee, S., Mellouki, A., Wang, W., 2016. Oxidative capacity and radical chemistry in the polluted atmosphere of Hong Kong and Pearl River Delta region: analysis of a severe photochemical smog episode. Atmos. Chem. Phys. 16, 9891–9903. https://doi.org/10.5194/acp-16-9891-2016.
Xue, C., Zhang, C., Ye, C., Liu, P., Catoire, V., Krysztofiak, G., Chen, H., Ren, Y., Zhao, X., Wang, J., Zhang, F., Zhang, C., Zhang, J., An, J., Wang, T., Chen, J., Kleffmann, J., Mellouki, A., Mu, Y., 2020. HONO budget and its role in nitrate formation in the rural North China Plain. Environ. Sci. Technol. 54, 11048–11057. https://doi.org/10.1021/acs.est.0c01832.
Xue, C., Ye, C., Zhang, C., Catoire, V., Liu, P., Gu, R., Zhang, J., Ma, Z., Zhao, X., Zhang, W., Ren, Y., Krysztofiak, G., Tong, S., Xue, L., An, J., Ge, M., Mellouki, A., Mu, Y., 2021. Evidence for strong HONO emission from fertilized agricultural fields and its remarkable impact on regional O3 pollution in the summer North China Plain. ACS EarthSpace Chem. 5, 340–347. https://doi.org/10.1021/acsearthspacechem.0c00314.
Yang, J., Shen, H., Guo, M.-Z., Zhao, M., Jiang, Y., Chen, T., Liu, Y., Li, H., Zhu, Y., Meng, H., Wang, W., Xue, L., 2021a. Strong marine-derived nitrous acid (HONO) production observed in the coastal atmosphere of northern China. Atmos. Environ. 244, 117948. https://doi.org/10.1016/j.atmosenv.2020.117948.
Yang, W., Han, C., Zhang, T., Tang, N., Yang, H., Xue, X., 2021b. Heterogeneous photochemical uptake of NO2 on the soil surface as an important ground-level HONO source. Environ. Pollut. 271. https://doi.org/10.1016/j.envpol.2020.116289.
Ye, C., Gao, H., Zhang, N., Zhou, X., 2016a. Photolysis of nitric acid and nitrate on natural and artificial surfaces. Environ. Sci. Technol. 50, 3530–3536. https://doi.org/10.1021/acs.est.5b05032.
Ye, C., Zhou, X., Pu, D., Stutz, J., Festa, J., Spolaor, M., Tsai, C., Cantrell, C., Mauldin III, R.L., Campos, T., Weinheimer, A., Hornbrook, R.S., Apel, E.C., Guenther, A., Kaser, L., Yuan, B., Karl, T., Haggerty, J., Hall, S., Ullmann, K., Smith, J.N., Ortega, J., Knote, C., 2016b. Rapid cycling of reactive nitrogen in the marine boundary layer. Nature 532, 489–491. https://doi.org/10.1038/nature17195.
Ye, C., Zhang, N., Gao, H., Zhou, X., 2017. Photolysis of particulate nitrate as a source of HONO and NOx. Environ. Sci. Technol. 51, 6849–6856. https://doi.org/10.1021/acs.est.7b00387.
Zha, Q., Xue, L., Wang, T., Xu, Z., Yeung, C., Louie, P.K.K., Luk, C.W.Y., 2014. Large conversion rates of NO2 to HNO2 observed in air masses from the South China Sea: evidence of strong production at sea surface? Geophys. Res. Lett. 41, 7710–7715. https://doi.org/10.1002/2014gl061429.
Zhang, S., Sarwar, G., Xing, J., Chu, B., Xue, C., Sarav, A., Ding, D., Zheng, H., Mu, Y., Duan, F., Ma, T., He, H., 2021. Improving the representation of HONO chemistry in CMAQ and examining its impact on haze over China. Atmos. Chem. Phys. 21, 15809–15826. https://doi.org/10.5194/acp-21-15809-2021.
Zhou, X., Zhang, N., Teravest, M., Tang, D., Hou, J., Bertman, S., Alaghmand, M., Shepson, P.B., Carroll, M.A., Griffith, S., Dusanter, S., Stevens, P.S., 2011. Nitric acid photolysis on forest canopy surface as a source for tropospheric nitrous acid. Nat. Geosci. 4, 440–443. https://doi.org/10.1038/ngeo1164.